

In-situ transport characterization of magnetic states in Nb/Co Superconductor/Ferromagnet heterostructures

Olena M. Kapran¹, Roman Morari^{2,3}, Taras Golod¹, Evgenii A. Borodianskyi¹, Vladimir Boian², Andrei Prepelita², Nikolay Klenov^{4,5}, Anatoli Sidorenko^{2,6,7} and Vladimir M. Krasnov^{1,3*}

¹ Department of Physics, Stockholm University, AlbaNova University Center, SE-10691 Stockholm, Sweden;

² Institute of Electronic Engineering and Nanotechnologies, MD2028 Chisinau, Moldova;

³ Moscow Institute of Physics and Technology, State University, 141700 Dolgoprudny, Russia;

⁴ Lomonosov Moscow State University Skobeltsyn Institute of Nuclear Physics, Moscow, 119991, Russia;

⁵ Moscow Technical University of Communication and Informatics, 111024 Moscow, Russia;

⁶ Laboratory of Functional Nanostructures, Orel State University named after I.S. Turgenev, 302026, Russia; and

⁷ Technical University of Moldova, MD2004, Chisinau, Moldova.

Employment of the non-trivial proximity effect in Superconductor/Ferromagnet (S/F) heterostructures for creation of novel superconducting devices requires an accurate control of magnetic states in complex thin-film multilayers. In this work we study experimentally in-plane transport properties of micro-structured Nb/Co multilayers. We apply various transport characterization techniques, including magnetoresistance, Hall effect and the first-order-reversal-curves (FORC) analysis. We demonstrate how FORC can be used for detailed *in-situ* characterization of magnetic states. It reveals that upon reduction of external field magnetization in ferromagnetic layers first rotates in a coherent scissor-like manner, then switches abruptly into the antiparallel state and after that splits into the polydomain state, which gradually turns into the opposite parallel state. The polydomain state is manifested by a profound enhancement of resistance caused by flux-flow phenomenon, triggered by domain stray fields. The scissor state represents the noncollinear magnetic state in which the unconventional odd-frequency spin-triplet order parameter should appear. The non-hysteric nature of this state allows reversible tuning of the magnetic orientation. Thus, we identify the range of parameters and the procedure for *in-situ* control of devices based on S/F heterostructures.

I. INTRODUCTION

Competition between spin-polarized ferromagnetism and spin-singlet superconductivity leads to a variety of interesting phenomena including possible generation of the odd-frequency spin-triplet order parameter [1–3]. In recent years this exotic state has been extensively studied both theoretically [4–18] and experimentally [19–35] in various Superconductor/Ferromagnet (S/F) heterostructures. It is anticipated, that this phenomenon can be employed for creation of novel superconducting devices, in which supercurrent is determined and controlled by the magnetic state of the heterostructure, i.e., by the relative orientation of magnetizations in several F-layers [19, 20, 23, 24, 26–36].

However, practical realization of such devices is complicated because neither ways of controlling many degrees of freedom in S/F multilayers, nor methods for monitoring magnetic states in micro- or nano-scale S/F devices are established. The situation is complicated by a variety of coexisting phenomena: (i) Both singlet and triplet currents with short and long-range components can flow through S/F heterostructures [12]. Therefore, even long-range supercurrent can not be automatically ascribed to the triplet order. (ii) Supercurrent strongly depends on a usually unknown domain structure in F [24, 31, 37], flux quantization in S [38, 39], both influenced by size and geometry. (iii) The long-range spin-triplet supercurrent appears only in the noncollinear magnetic state [5, 9–

12]. Therefore, utilization of this phenomenon for device applications requires accurate determination and control of the micromagnetic state of micro- or nano-scale devices. A similar control is needed for operation of a large number of superconducting spintronics devices, including memory elements and spin valves [23, 30, 35, 40–44]. The need for establishing experimental characterization techniques for *in-situ* monitoring of magnetic states in S/F micro and nano-devices is our main motivation.

Here we study experimentally in-plane transport properties of micro-structured Nb/Co multilayers (ML's) with different number of layers and layer thicknesses. Our goal is to demonstrate how conventional experimental techniques can be used for *in-situ* assessment of magnetic states of small S/F devices. The key technique that we employ is the first-order-reversal-curves (FORC) analysis. We demonstrate that in combination with magnetoresistance (MR) and Hall effect measurements, it can provide a detailed knowledge of the magnetic configuration in the ML. In particular we identify the parallel (P), the antiparallel (AP), the noncollinear monodomain scissor-state and polydomain states. We observe that the domain state is manifested by a profound enhancement of resistance. Analysis of the Hall effect reveals that those maxima are associated with flux-flow phenomenon, caused by motion of Abrikosov vortices induced by domain stray fields. From device application perspective, the most important is the noncollinear scissor state, in which the unconventional odd-frequency spin-triplet order parameter should appear. The non-hysteric nature

of this state allows reversible tuning of the magnetic configuration. Thus, we identify the range of parameters and the procedure for controllable operation of devices based on S/F heterostructures.

II. SAMPLES

We study two types of Nb/Co ML's with different number of layers and layer thicknesses. The simplest S1: Nb(50 nm)/Co(1.5 nm)/Nb(8 nm)/Co(2.5 nm)/Nb(8 nm)/Si ML (bottom -to -top), has just two dissimilar Co layers composing a single pseudo spin valve. A more complex S2: Nb(50 nm)/[Co(1.5 nm)/Nb(6 nm)/Co(2.5 nm)/Nb(6 nm)]₃Co(1.5 nm)/Nb(6 nm)/Si (the structure in square brackets is repeated three times) has five Co layers. ML's are deposited by magnetron sputtering in a single deposition cycle without breaking vacuum. We use Nb target (99.95 % purity) for deposition of S-layers, Co (99.95 % purity) for F-layers, and Si (99.999 %) for seeding bottom and protective top layers. ML's are grown on a (1 1 1) Si wafers. Prior to deposition, targets were precleaned by plasma-etching for 3 minutes and in addition for 1 minute upon switching between targets. The deposition is performed at room temperature with water cooled sample stage. Thicknesses are defined using calibrated growth rates: 3.5 nm/s for Nb and 0.1 nm/s for Co. For every set of layers, three identical samples were prepared simultaneously, of which some were used for calibration of films etching rates. ML's are patterned into micron-scale bridges with multiple contacts using photolithography and reactive ion etching. Scanning electron microscope (SEM) image of one of the studied samples is shown in Fig. 1 (a).

Control of the magnetic state implies a possibility of variation of a relative magnetization orientation in neighbor F-layers, which requires different coercive fields. To facilitate this we use dissimilar Co layers with thicknesses 1.5 and 2.5 nm. Nb/Co ML's with similar Co thicknesses have been studied earlier and demonstrated good uniformity and perspectives for device applications [26, 27, 29, 33, 34, 44, 45]. Fig. 1 (b) shows a magnetization curve for a similar Nb(25 nm)/[Co(1.5 nm)/Nb(8 nm)/Co(2.5 nm)/Nb(8 nm)]₆Co(1.5 nm)/Nb(25 nm) unpatterned ML film, deposited using the same setup (data from Ref. [44]). $M(H)$ is obtained by SQUID magnetometer in field parallel to the film in the normal state, $T > T_c$. A significant hysteresis of $M(H)$ reveals the in-plane anisotropy of Co films (albeit with a small coercive field, $H_C \sim 30$ Oe), consistent with earlier studies [45–48].

Fig. 1 (c) shows numerical simulation of the superconducting order parameter, Δ , distribution in S/F ML similar to S2 [49]. It provides a qualitative understanding of modulation of the proximity effect in the ML in P (red) and AP (blue) states. A thick bottom S-layer

Nb(50 nm) acts as a Cooper pair reservoir and is only modestly affected by F-layer orientation. However, thin S' spacers, Nb(6 and 8 nm), with the thickness comparable to the superconducting coherence length, $\xi_S \sim 10$ nm, are strongly affected. Superconductivity in S' layers is stronger in the AP-state and is almost quenched in the outmost S' layer in the P-state. This demonstrates the tunability of superconductivity in such S/F ML's by changing the magnetic state. Because of the bottom S-layer, there is a gradient of Δ in S' layers, which implies that S' layers have dissimilar superconducting properties.

Measurements are performed in a closed-cycle ³He cryostat with a superconducting magnet. More details about fabrication, characterization and experimental setup can be found elsewhere [24, 35, 44]. Resistances are measured by the lock-in technique with different current amplitudes I_{ac} . In all cases magnetic field is applied parallel to the film plane in the orientation, sketched in Fig. 1 (g). Multi-terminal geometry of samples allows simultaneous four-probe measurements of different segments of the sample in both longitudinal, R_{xx} , and Hall, R_{xy} , directions. When current is sent through the central vertical bridge, as sketched in Fig. 1 (g), measurements correspond to the easy-axis magnetization orientation (field along the long side of the vertical line). Alternatively we can send current through horizontal bridges, which corresponds to the hard-axis magnetization orientation (field perpendicular to the long side of the bridge).

III. RESULTS

Fig. 1 (d) shows $R_{xx}(T)$ dependencies, normalized by the normal state resistance $R_n(T > T_c)$, for microbridges at S1 (blue) and S2 (red) ML's at $H = 0$. Resistances are measured with $I_{ac} = 10 \mu\text{A}$ for S1 and $20 \mu\text{A}$ for S2, which correspond to approximately equal small current densities in both ML's. Both ML's show a double transition, which could be attributed to different critical temperatures in S and S' layers, $T'_c(S') < T_c(S)$. Consistent with this assumption, T'_c of the S2 ML with thinner S'(6 nm) is smaller than for S1 ML with S'(8 nm).

Fig. 1 (e) shows $R_{xx}(T)$ curves for a horizontal bridge at the S1 sample at four sequentially increasing magnetic fields (hard-axis orientation) and $I_{ac} = 1$ mA. It is seen that the onset of resistivity at $T \sim 7.3$ K is affected by the field. However, this effect is nonmonotonous with field, as can be seen from the zoomed-in view in the inset. The rest of transition is little affected in this field range $\lesssim 500$ Oe. This is caused by the large value of the upper critical field for thin Nb films in parallel field [50]. Therefore, the observed nonmonotonous field dependence is not directly induced by the applied field but reflects the remagnetization process of F-layers in the ML.

Fig. 1 (f) shows the $R_{xx}(T)$ curve for a horizontal bridge at the S2 sample (hard axis orientation), measured

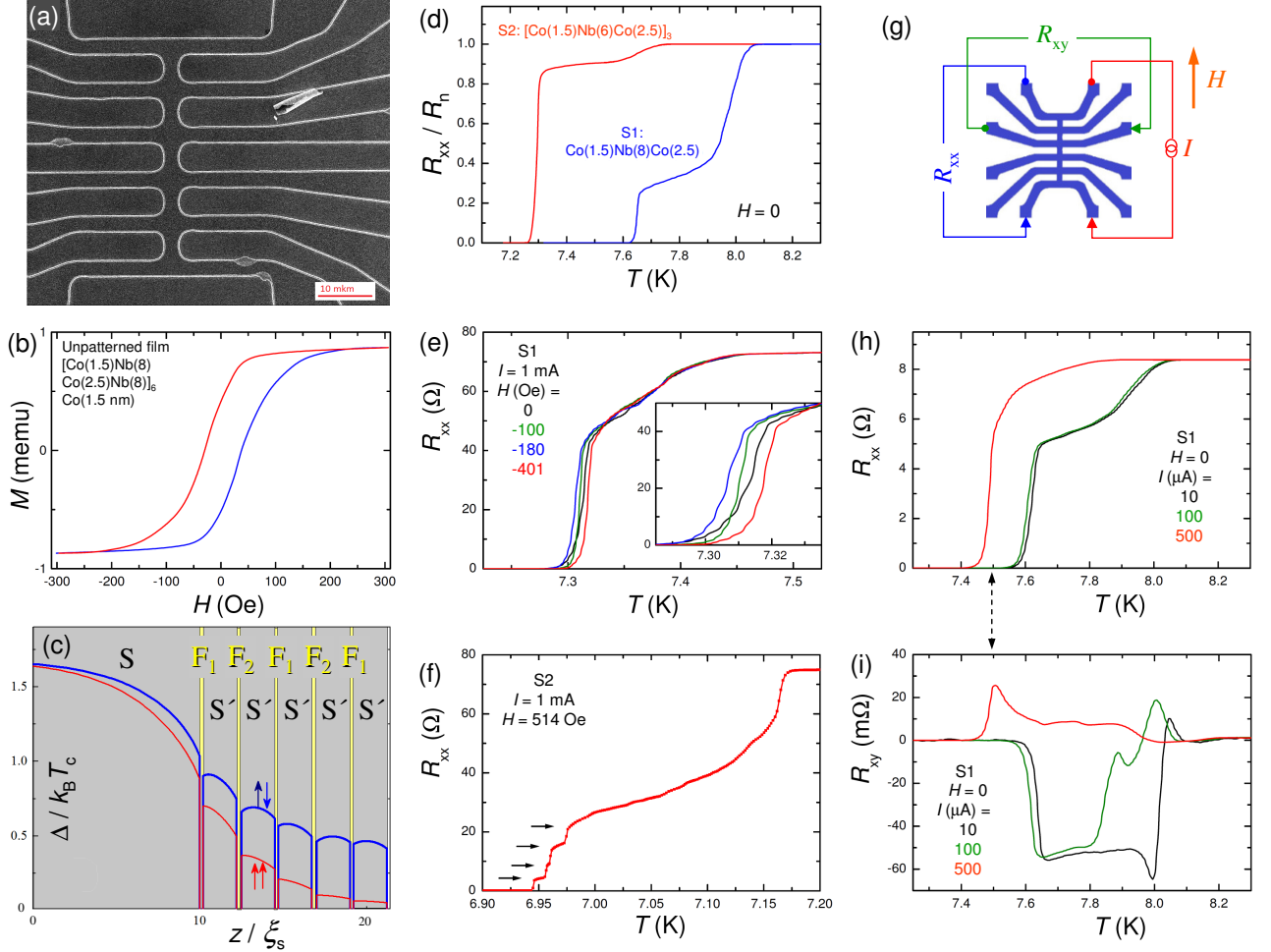


FIG. 1. (color online). (a) SEM image of a micro-patterned Nb/Co multilayer. The sample contains 12 contacts, six horizontal and one vertical bridge with the widths of few microns. (b) Magnetization curve of an unpatterned Nb(25)[Co(1.5)Nb(8)Co(2.5)Nb(8)]₆Co(1.5 nm)Nb(25) ML. Blue/red curves represent up/down field sweeps (data from Ref.[44]). (c) Simulated superconducting energy gap, Δ , in the S2 ML for P (red) and AP (blue) states. (d) Temperature dependencies of longitudinal resistances, normalized by $R_n(T \gtrsim T_c)$, for both ML's. Measurements are taken with small currents at $H = 0$. Double transitions are attributed to different critical temperatures of thick bottom S-layer and thin S'-spacers. (e) $R_{xx}(T)$ for a horizontal bridge (S1) at four consecutively increasing fields and $I_{ac} = 1$ mA. Inset demonstrates a nonmonotonous dependence on magnetic field. (f) $R_{xx}(T)$ for a horizontal bridge (S2) at $H = 514$ Oe and $I_{ac} = 1$ mA. The resistive transition is significantly broadened, compared to the case in (d). Several small steps (marked by arrows) with similar resistance increments are seen. (g) Contact configuration for measurement of longitudinal and Hall resistances for (h) and (i) and the orientation of magnetic field in all experiments. (h) Longitudinal and (i) Hall resistances for a vertical bridge at S1 sample at different bias currents and $H = 0$. A significant and sign-reversal Hall signal is observed within the transition region. This is a fingerprint of a flux-flow phenomenon, caused by motion of Abrikosov vortices in S-layers.

at $H = 514$ Oe with $I_{ac} = 1$ mA. Here several steps (marked by arrows) with similar resistance increments $\sim 5 \Omega$ can be distinguished close to the onset of $R_{xx}(T)$. They are probably due to individual transitions of five S' layers in this ML, which have a gradient of the order parameter, as seen from Fig. 1 (c).

III A. Non-linear flux-flow Hall effect

Resistivity in type-II superconductors with sizes significantly larger than the London penetration depth, λ , is caused by motion of Abrikosov vortices, i.e., has a flux-flow (FF) nature [52–55]. Since our micron-size bridges are significantly larger than $\lambda \sim 100$ nm of Nb, the FF phenomenon is anticipated. FF depends on magnetic field, transport current and vortex pinning, which depends on temperature. For a single S-layer at $H = 0$

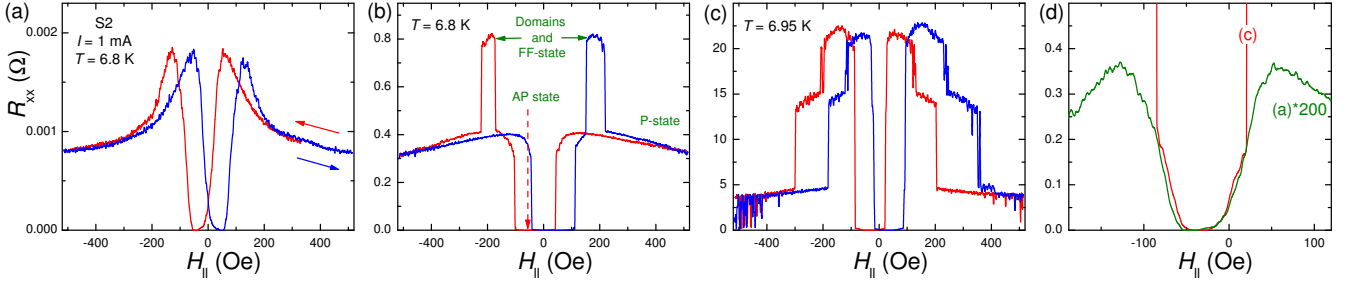


FIG. 2. (color online). Longitudinal magnetoresistances for a horizontal bridge at S2, measured at different T . (a) At the lowest $T \simeq 6.8$ K, corresponding to the very onset of resistivity. (b) At marginally higher T . Here an additional maximum appears, which is attributed to triggering of the flux-flow phenomenon by domain. (c) At $T \simeq 6.95$ K, corresponding to the middle of the resistive transition, shown in Fig. 1 (f). Steps are attributed to transitions of individual spacer layers. (d) Low-resistance parts of the curves from (a) and (c), which demonstrate a similar behavior in the AP-state.

vortices may only be induced by the self-field of transport current. However, for S/F heterostructures they may also be induced by stray fields from F-layers, especially in the presence of domain walls [56–59]. Domain walls also affect the FF phenomenon because they create a pinning landscape for vortices: vortices are pinned to domains and can not move across them, but can freely move along domain walls [57]. Therefore, we expect that the magnetic state of a ML may influence FF resistance.

Fig. 1 (h) shows $R_{xx}(T)$ for a vertical bridge at S1 sample with contact configuration depicted in Fig. 1 (g). All the curves are obtained at $H = 0$, without remagnetizing the ML. However, measurements are made with different current amplitudes I_{ac} : 10 μ A (black), 100 μ A (olive) and 500 μ A (red). At low and intermediate bias currents, 10 and 100 μ A, a two-step $R_{xx}(T)$ transition occurs with $T_c(S) \simeq 8$ K and $T'_c(S') \simeq 7.8$ K and the shape of $R_{xx}(T)$ is remaining the same. This indicates that the current-voltage characteristics at low bias is almost linear and resistance is almost bias independent. However, at high bias, $I_{ac} = 500$ μ A, the $R_{xx}(T)$ is significantly smeared out and the onset shifts to significantly lower T . This manifests entrance into the non-linear regime.

Fig. 1 (i) shows corresponding Hall resistances measured as shown in Fig. 1 (g). It is seen that a significant Hall signal appears only within the resistive transition region [51] and is non-linear (bias-dependent) even at low bias. Furthermore, at low and intermediate bias R_{xy} changes sign. Such a behavior is typical for the FF Hall effect in superconductors [52–54]. This provides clear evidence for FF phenomenon in our samples. From comparison of Figs. 1 (h) and (i) it is clear that FF takes place in the whole resistive transition region.

III B. Flux-flow magnetoresistance, triggered by domains

Figure 2 shows longitudinal magnetoresistances at different temperatures. Measurements are done on a horizontal bridge (hard axis orientation) at the S2 sample, the same as in Fig. 1 (f), and at the same current $I_{ac} = 1$ mA. Blue/red lines represent up/down field sweeps. The curves in Fig. 2 (a) are measured at the very onset of the resistive transition, as seen from small (m Ω) resistance values. Here we observe the simplest MR curves, most consistent with the two-state theoretical prediction based on mono-domain simulations, as in Fig. 1 (c). Namely, P state at high field with large R_{xx} (suppressed superconductivity) and AP state at low fields with small R_{xx} (enhanced superconductivity) [4–6, 8–10, 21, 33, 35, 36]. However, this simple scenario does not explain appearance of additional maxima between P and AP states. The discrepancy becomes more pronounced at higher T , i.e., higher up at the $R_{xx}(T)$ transition.

Fig. 2 (c) shows MR at almost the same T as in (a) with a higher, but still quite small $R_{xx} < 1$ Ω . Fig. 2 (c) represents MR at higher T , corresponding to the middle of the first transition in $R_{xx}(T)$ from Fig. 1 (f). Here the maxima between P-state (high fields) and AP state ($R_{xx} \simeq 0$ at low fields) become profound. Appearance of such a maximum also follows from the non-monotonous field variation of $R_{xx}(T)$ curves, as can be seen from the inset in Fig. 1 (e). In Fig. 2 (c) it is seen that the resistance switches stepwise between certain values $\sim 0, 5, 10$ (missing in (c), but accessible at slightly different T), 15 and 20 Ω . They correspond to steps in $R_{xx}(T)$ indicated in Fig. 1 (f), which we attributed to transition of individual S' layers. From Figs. 1 (b) and (c) it can be seen that the fields at which resistance drops slightly depends on T . This does not allow a straightforward association of such the drop with transition into the AP state, which should be T -independent in this T -range.

In Fig. 1 (d) we replot low-field parts of the downward

curves from (a) and (c). It is seen that they coincide after proper scaling, i.e. they represent T -independent part of MR, which could be associated with the magnetic state. In this case the minima with $R_{xx} \simeq 0$ from -20 to -50 Oe should represent the range of existence of the AP state. Observation of this scaling points out that the underlying magnetic state is independent of T and the difference in shapes of MR is caused by something else. The origin of the observed unusual three-state MR with an additional profound maximum between AP and P states is not difficult to deduce. The third magnetic state is very well known - the polydomain state. It for sure appears in micron-scale F-films. Since the resistivity of thin S-films has FF origin, the observed unusual maximum in MR is likely caused by triggering of FF phenomenon by domain stray fields, which change upon remagnetization of F-layers. The remarkable temperature variation of MR in Figs. 2 (a-c) is then primarily caused by temperature variation of vortex mobility.

III C. *In-situ* characterization of magnetic states by the first-order-reversal-curves analysis

The aim of this work is to establish techniques for *in-situ* transport characterization of magnetic states in micro-patterned S/F ML's. The key technique that we employ for this purpose is FORC - a powerful tool for characterization of magnetic states in complex ferromagnetic structures [60–62]. FORC analysis starts at the same saturated state. Then field is swept to a reversal field H_r and measurements are carried out on the way back to the saturated state. The experiment is repeated with gradually varying H_r . Recently it has been shown that FORC can be used for the analysis of magnetic states in S/F ML's [35]. Essentially we have to search for appearance of different types of hysteresis in the FORC response, which indicate switching into some specific metastable magnetic states. There are two mechanisms for appearance of hysteresis in the ML's [35, 38]. The major hysteresis is associated with switching in and out from the magnetostatically stable AP state. Multiple smaller ones are associated with switching between different domain states, which are also metastable.

Fig. 3 (a) shows longitudinal MR for the same horizontal bridge (hard axis orientation) at S1 sample as in Fig. 1 (e). The overall shape of $R_{xx}(H)$ with a minimum at low fields and an additional FF maximum nearby is similar to that for S2 in Fig. 2 (b). Fig. 3 (b) represents FORC analysis for this bridge. Magnetic field is swept from above the saturation field $H \simeq +500$ Oe down to the reversal field H_r and back to the saturation field. Red lines represent forward curves and blue - the FORC's. For $H_r \simeq +14$ Oe, curve-1 in Fig. 3 (b), the FORC is reversible. The non-hysteretic behavior corresponds to coherent monodomain rotation of magnetization in a

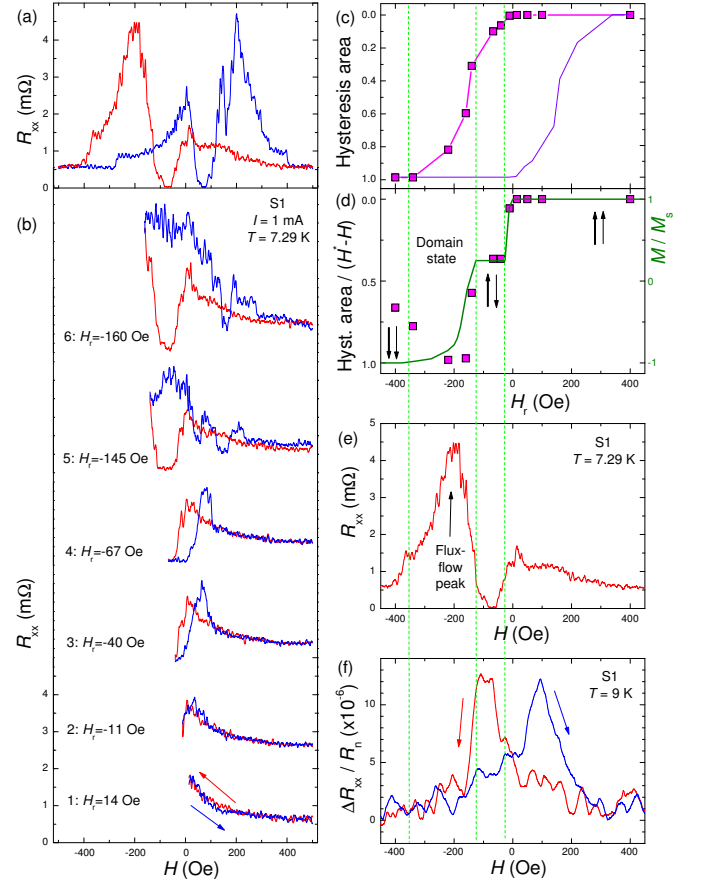


FIG. 3. (color online). (a) Magnetoresistance of a horizontal bridge on the S1 sample at $T = 7.29$ K. (b) FORC analysis of MR for different reversal fields H_r (curves are shifted vertically for clarity). (c) Hysteresis area between forward (red) and reversal (blue) curves in (b). Violet curve shows a central-symmetric reflection of the same data. (d) Hysteresis area normalized by the integration field range $H^* - H_r$, where H^* is the field for onset of the hysteresis. Olive line (right axis) represents a sketch of the expected magnetization curve. (e) Full-scale $R_{xx}(H)$ curve at $T = 7.29$ K for a downward field sweep. (f) Normal state magnetoresistance $(R_{xx}(H) - R_n)/R_n$ for the same bridge at $T = 9$ K. Green vertical lines emphasize correlations between features in (c-f).

scissor-like manner [35, 38]. At $H_r = -11$ Oe, curve-2, the FORC starts to show a tiny signature of hysteresis, which disappears at $H > 50$ Oe. For $H_r \simeq -40$ Oe, curve-3, the forward (red) curve reached the minimum $R_{xx} \simeq 0$, characteristic for the AP state, and the reversal curve (blue) start to exhibit a clear hysteresis. With further increase of H_r within the minimum the reversal curve is practically unchanged, as seen from the curve-4. This indicates that the state of the ML remains the same. As reported in Ref. [35] appearance of the initial hysteresis at small fields is associated with switching to the AP state. This is fully consistent with our observation that the initial hysteresis corresponds to the minimum of R_{xx} .

With further increase of H_r , beyond the AP minimum, the reversal curve clearly changes, see curve-5, indicating switching into a different magnetic state. Furthermore the range of hysteresis expands to $H > 200$ Oe and several additional small switches occur within this range. The curve-6 in Fig. 3 (b) is obtained for $H_r = -160$ Oe in the middle of the R_{xx} maximum. The reversal curve is clearly different from curve-5 revealing yet another initial state. With further increase of H_r towards the negative saturation field, the hysteresis changes gradually until reaching the saturated state, shown in Fig. 3 (a). Such a gradual transformation indicates that the ML is in a polydomain state with many close metastable states.

For a more quantitative analysis of FORC data, following Ref. [35], in Fig. 3 (c) we plot H_r -dependence of normalized hysteresis area between forward and reverse curves, i.e. the integral of the absolute value of the difference between red and blue curves in Fig. 3 (b). Magenta symbols represent FORC data. They are plotted in a reverse scale along the vertical axis to resemble magnetization curves. From this plot it is clearly seen how the hysteresis start to develop at $H_r \lesssim -10$ Oe and saturates at $H_r \lesssim -350$ Oe. However, this curve does not represent the magnetization curve. In particular, at the AP minimum in the range $-120 \text{ Oe} \lesssim H_r \lesssim -20 \text{ Oe}$ the state of the ML remains the same, as follows from the similarity of FORC curves 3 and 4 in Fig. 3 (b). In this range the hysteresis area is growing linearly with H_r simply because the integration range is increasing as $H^* - H_r$, where H^* is the field for onset of hysteresis. In Fig. 3 (d) we plot hysteresis area divided by $H^* - H_r$. With such a normalization the AP state is properly described by a plateau. For comparison we also show a sketch of the expected magnetization curve (olive line, right axis), with the AP plateau at $0.25 = (2.5\text{nm} - 1.5\text{nm}) / (2.5\text{nm} + 1.5\text{nm})$ of the saturation magnetization M_s . It is seen that such representation provides a remarkably close description of $M(H)$ curves at intermediate fields. At higher fields $H < -220$ Oe the points start to fall down, which indicates approaching to the saturation state at which the hysteresis area is no longer depending on the integration range $H^* - H_r$, as seen from Fig. 3 (c).

For completeness of the analysis, in Figs. 3 (e) we replot the full MR curve and in Fig.3 (f) show the normal-state MR for the same bridge at $T = 9$ K. The two rightmost vertical lines in (c-f) marks the onset and the end of the AP state. The leftmost vertical line marks the onset of the saturation. The two rightmost lines emphasize a clear correlation between the onset of hysteresis (c,d), the minimum of resistance in the superconducting state (e) and the maximum of resistance in the normal state (f), which all are signatures of the AP state. The two leftmost vertical lines indicate correlations between the FF maximum in R_{xx} (e) and a gradual transition state between the AP state and the negative P-state (d,f).

Thus, from FORC analysis we conclude that upon re-

magnetization of the ML from the P-state, it first enters into a coherently rotating, nonhysteretic, scissor state, after which it abruptly switches into the AP state, stays in it for a while and then breaks into a polydomain state, which triggers the flux-flow phenomenon. With further increase of field the polydomain state gradually turns into the opposite P-state. This picture is consistent with the assessment based on Hall effect, Fig. 1 (i), and MR analysis, Fig. 2, and with earlier FORC analysis of Ni-based $\text{SF}_1\text{NF}_2\text{S}$ spin valves [35].

IV. DISCUSSION

As we've seen, information about evolution of magnetic states in S/F ML's is encoded in the shapes of MR curves. The most remarkable feature of those is the three-state remagnetization with an unusual maximum in addition to well understood P and AP states. As we already mentioned, the third state has to be the well known polydomain state. Below we substantiate this statement.

First, we note that resistance in our films has the flux-flow origin, as unambiguously shown by Hall effect measurements, Fig. 1 (i). Therefore, MR is due to modulation of FF. The latter depends on the vortex density, pinning, the superconducting order parameter and the driving current. Next, we can do the following exclusion:

(i) Vortices in thin films have a pancake structure (Pearl vortices) with field perpendicular to the film. Therefore, vortex density depends on magnetic induction B_z perpendicular to the film. Since the applied field in our experiment is parallel to the film, it does not contribute to B_z .

(ii) Parallel magnetic field does suppress superconductivity. However, it should cause a monotonous (parabolic) increase of R_{xx} with increasing field, which is not the case. Thus, field variation as such does not explain the observed nonmonotonous MR.

(iii) Since all measurements in Fig. 2 are done with the same $I_{ac} = 1$ mA, the current self-field is not changing and, therefore, can not cause modulation of MR.

The above exclusion leaves one possible source of MR specific for S/F ML's: variation of magnetic state in F-layers. However, remagnetization of F-layers can contribute to flux-flow phenomenon only if it generates the perpendicular field component. Since our Co layers have the in-plane anisotropy, this is only possible via stray fields from domain walls [56–59]. This brings us to the following interpretation of the observed unusual MR, as indicated in Fig. 2 (b): MR modulation has two contributions: First is the conventional suppression/enhancement of superconductivity (order parameter modulation) in the P/AP states at high/small fields [4–6, 8–10, 21, 33, 35, 36]. The second contribution is caused by the flux-flow phenomena triggered by domains. Domains both create vortices and generate a pinning land-

scape that determines the direction of vortex motion [57]. Domains could explain the observed dramatic variation of MR shapes with T : at low T , Fig. 2 (a), FF is negligible (vortices are almost immobile) and the MR is dominated by order parameter modulation, leading to appearance of a minimum at low fields. With increasing T vortices get depinned and FF modulated by domain texture becomes a dominant factor, causing appearance of additional maxima in-between P and AP states as in Figs. 2 (b,c).

Generally, the polydomain state is unwanted in most devices based on S/F heterostructures because it is hard to control. Domains cause an irreversible behavior of the heterostructure, associated with both the magnetic hysteresis and with generation of Abrikosov vortices, which are pinned at film defects. As shown previously [24], those two factors may dramatically distort characteristics of S/F devices.

FORC is the key technique, that we are advertising for *in-situ* transport characterization of magnetic states. As shown in sec. III C and in Ref. [35], FORC may provide a detailed information about variation of magnetic states in micro and nano-scale S/F devices. In Ref. [35] this was demonstrated using out-of-plane measurements. Here we show that a similar information can be obtained using in-plane transport measurements. From FORC analysis in Figs. 3 we can characterize evolution of micromagnetic states in our structures upon remagnetization. We observe that the initial stage of remagnetization from P to AP state is fully reversible, see curve-1 in Figs. 3 (b). Micromagnetic simulations show that such stage corresponds to monodomain coherent rotation of magnetizations in neighbor F-layers in opposite directions in a scissor-like manner [35, 38]. As seen from Fig. 3 (d), the hysteresis appears abruptly upon switching into the AP-state. The AP-state is magnetostatically stable and, therefore persists in a certain field range. However, switching from AP to the opposite P-state occurs gradually, which according to micromagnetic simulations indicate splitting into polydomain state [35, 38]. The more domains - the more gradual is the transition to the saturated state. Appearance of domains triggers the flux-flow state by introducing Abrikosov vortices, as reported before [57–59] and leads to appearance of the additional FF-maximum in MR.

CONCLUSIONS

To conclude, we have studied in-plane transport properties of micro-structured Nb/Co multilayers. We demonstrated how conventional transport techniques can be used for assessment of magnetic states of small S/F heterostructures and devices. For this we apply various experimental techniques, including magnetoresistance, Hall effect and first-order-reversal-curves analysis. We have shown that a combination of those techniques,

performed simultaneously, can provide a detailed knowledge about evolution of micro-magnetic states. FORC is the key technique that we advertise for such *in-situ* characterization. Using it we identified the parallel, the antiparallel, the mono-domain scissor-state and polydomain states. Polydomain states are manifested by a profound enhancement of resistance caused by flux-flow phenomenon, triggered by domain stray fields.

Importantly, the scissor state corresponds to the non-collinear magnetic state of the multilayer in which the unconventional odd-frequency spin-triplet order parameter should appear in the heterostructure. The non-hysteretic nature of this state allows controllable tuning of magnetic orientation. Thus, we identify the range of parameters and the procedure for controllable operation of superconducting spintronic devices based on S/F heterostructures. Essentially we conclude that for moderately small (micrometer-scale) devices controllable and highly reversible operation can be achieved at fields between one of the P-states down to the AP state without entering into the realm of the opposite P state.

Acknowledgments

We are grateful to Sergey Bakurskiy, Igor Soloviev, Andrey Schegolev, Yury Khaydukov, Mikhail Kupriyanov and Alexander Golubov for stimulating discussions. The work was supported by the European Union H2020-WIDESPREAD-05-2017-Twinning project “SPINTECH” under grant agreement Nr. 810144 (sample preparation and low temperature measurements), the Russian Science Foundation grant No. 19-19-00594 (V.M.K.: data analysis and manuscript preparation), and partially by the project STCU #6329 “Full switching memory element for spintronics on the base of superconducting spin-valve effect” (A.S.). The manuscript was written during a sabbatical semester of V.M.K. at MIPT, supported by the Faculty of Natural Sciences at SU and the Russian Ministry of Education and Science within the program “5top100”.

* E-mail: Vladimir.Krasnov@fysik.su.se

- [1] A. I. Buzdin, A. V. Vedyayev, and N. V. Ryzhanova, Spin-orientation-dependent superconductivity in F/S/F structures. *Europhys. Lett.* **54**, 686-691 (1999).
- [2] A. Kadigrobov, R. I. Shekhter, and M. Jonson, Quantum spin fluctuations as a source of long-range proximity effects in diffusive ferromagnet-superconductor structures. *Europhys. Lett.* **48**, 394-400 (2001).
- [3] F. S. Bergeret, A. F. Volkov, and K. B. Efetov, Long-range proximity effects in superconductor-ferromagnet structures. *Phys. Rev. Lett.* **86**, 4096-4099 (2001).

- [4] A. I. Buzdin, Proximity effects in superconductor-ferromagnet heterostructures. *Rev. Mod. Phys.* **77**, 935-976 (2005).
- [5] F. S. Bergeret, A. F. Volkov, and K. B. Efetov, Odd triplet superconductivity and related phenomena in superconductor-ferromagnet structures. *Rev. Mod. Phys.* **77**, 1321-1373 (2005).
- [6] Ya. V. Fominov, A. A. Golubov, T. Yu. Karminskaya, M. Yu. Kupriyanov, R. G. Deminov, and L. R. Tagirov, Superconducting Triplet Spin Valve. *JETP Lett.* **91**, 308 (2010).
- [7] Ya.M. Blanter and F.W.J. Hekking, Supercurrent in long SFFS junctions with antiparallel domain configuration. *Phys. Rev. B* **69**, 024525 (2004).
- [8] M. Eschrig, Spin-polarized supercurrents for spintronics: a review of current progress. *Rev. Prog. Phys.* **78**, 104501 (2015).
- [9] M. Houzet and A.I. Buzdin, Long range triplet Josephson effect through a ferromagnetic trilayer. *Phys. Rev. B* **76**, 060504(R) (2007).
- [10] Y. Asano, Y. Sawa, Y. Tanaka, and A.A. Golubov, Odd triplet superconductivity and related phenomena in superconductor-ferromagnet structures. *Phys. Rev. B* **76**, 224525 (2007).
- [11] L. Trifunovic, Z. Popovic, and Z. Radovic, Josephson effect and spin-triplet pairing correlations in SF1F2S junctions. *Phys. Rev. B* **84**, 064511 (2011).
- [12] A.S. Mel'nikov, A.V. Samokhvalov, S.M. Kuznetsova, and A.I. Buzdin, Interference Phenomena and Long-Range Proximity Effect in Clean Superconductor-Ferromagnet Systems. *Phys. Rev. Lett.* **109**, 237006 (2012).
- [13] N.G. Pugach, and A.I. Buzdin, Magnetic moment manipulation by triplet Josephson current. *Appl. Rev. Lett.* **101**, 242602 (2012).
- [14] M. Alidoust, G. Sewell, and J. Linder, Non-Fraunhofer Interference Pattern in Inhomogeneous Ferromagnetic Josephson Junctions *Phys. Rev. Lett.* **108**, 037001 (2012).
- [15] C. Richard, A. Buzdin, M. Houzet, and J.S. Meyer, Signatures of odd-frequency correlations in the Josephson current of superconductor/ferromagnet hybrid junctions, *Phys. Rev. B* **92**, 094509 (2015).
- [16] S. Hikino and S. Yunoki, Magnetization induced by odd-frequency spin-triplet Cooper pairs in a Josephson junction with metallic trilayers. *Phys. Rev. B* **92**, 024512 (2015).
- [17] J. Linder and J. W. A. Robinson, Superconducting spintronics. *Nature Phys.* **11**, 307 (2015).
- [18] H. Meng, J. Wu, X. Wu, M. Ren, and Y. Ren, Long-range superharmonic Josephson current and spin-triplet pairing correlations in a junction with ferromagnetic bilayers. *Sci. Rep.* **6**, 21308 (2016).
- [19] C. Bell, G. Burnell, C.W. Leung, E.J. Tarte, D.-J. Kang, and M.G. Blamire, Controllable Josephson current through a pseudospin-valve structure. *Appl. Rev. Lett.* **84**, 1153-1155 (2004).
- [20] J.W.A. Robinson, G.B. Halász, A.I. Buzdin, and M.G. Blamire, Enhanced Supercurrents in Josephson Junctions Containing Nonparallel Ferromagnetic Domains, *Phys. Rev. Lett.* **104**, 207001 (2010).
- [21] P. V. Leksin, N. N. Garif'yanov, I. A. Garifullin, J. Schumann, V. Kataev, O. G. Schmidt, and B. Büchner, Manifestation of New Interference Effects in a Superconductor-Ferromagnet Spin Valve. *Phys. Rev. Lett.* **106**, 067005 (2011).
- [22] V.I. Zdravkov, J. Kehrle, G. Obermeier, D. Lenk, H.-A.K. von Nidda, C. Mueller, M.Y. Kupriyanov, A.S. Sidorenko, S. Horn, R. Tidecks, and L.R. Tagirov, Experimental observation of the triplet spin-valve effect in a superconductor-ferromagnet heterostructure. *Phys. Rev. B* **87**, 144507 (2013).
- [23] B. Baek, W.H. Rippard, S.P. Benz, S.E. Russek, and P.D. Dresselhaus Hybrid superconducting-magnetic memory device using competing order parameters *Nat. Commun.* **5**, 3888 (2014).
- [24] A. Iovan, T. Golod, and V. M. Krasnov, Controllable generation of a spin-triplet supercurrent in a Josephson spin valve, *Phys. Rev. B* **90**, 134514 (2014).
- [25] Yu. N. Khaydukov, G. A. Ovsyannikov, A. E. Sheyerman, K. Y. Constantinian, L. Mustafa, T. Keller, M. A. Uribe-Laverde, Yu. V. Kislinkii, A. V. Shadrin, A. Kalaboukhov, B. Keimer, and D. Winkler, Evidence for spin-triplet superconducting correlations in metal-oxide heterostructures with noncollinear magnetization, *Phys. Rev. B* **90**, 035130 (2014).
- [26] J. W. A. Robinson, J. D. S. Witt, and M. G. Blamire, Controlled Injection of Spin-Triplet Supercurrents into a Strong Ferromagnet, *Science* **329**, 59 (2010).
- [27] T.S. Khaire, M.A. Khasawneh, W.P. Pratt, Jr., and N.O. Birge, Observation of Spin-Triplet Superconductivity in Co-Based Josephson Junctions. *Phys. Rev. Lett.* **104**, 137002 (2010).
- [28] N. Banerjee, J.W.A. Robinson and M.G. Blamire, Reversible control of spin-polarized supercurrents in ferromagnetic Josephson junctions. *Nature Commun.* **5**, 4771 (2014).
- [29] W. M. Martinez, W. P. Pratt, Jr., and N. O. Birge, Amplitude Control of the Spin-Triplet Supercurrent in S/F/S Josephson Junctions. *Phys. Rev. Lett.* **116**, 077001 (2016).
- [30] J. A. Glick, V. Aguilar, A. B. Gougam, B. M. Niedzielski, E. C. Gingrich, R. Loloee, W. P. Pratt Jr., and N. O. Birge, Phase control in a spin-triplet SQUID. *Sci. Adv.* **4**, eaat9457 (2018).
- [31] K. Lahabi, M. Amundsen, J. A. Ouassou, E. Beukers, M. Pleijster, J. Linder, P. Alkemade, and J. Aarts. Controlling supercurrents and their spatial distribution in ferromagnets. *Nature Commun.* **8**, 2056 (2017).
- [32] O. Vávra, R. Soni, A. Petraru, N. Himmel, I. Vávra, J. Fabian, H. Kohlstedt, and Ch. Strunk, Coexistence of tunneling magnetoresistance and Josephson effects in SFIFS junctions. *AIP Adv.* **7**, 025008 (2017).
- [33] D. Lenk, V. I. Zdravkov, J.-M. Kehrle, G. Obermeier, A. Ullrich, R. Morari, H.-A. Krug von Nidda, C. Müller, M. Yu. Kupriyanov, A. S. Sidorenko, S. Horn, R. G. Deminov, L. R. Tagirov and R. Tidecks, Thickness dependence of the triplet spin-valve effect in superconductor-ferromagnet-ferromagnet heterostructures. *Beilstein J. Nanotechnol.* **7**, 957 (2016).
- [34] D. Lenk, R. Morari, V. I. Zdravkov, A. Ullrich, Yu. Khaydukov, G. Obermeier, C. Müller, A. S. Sidorenko, H.-A. Krug von Nidda, S. Horn, L. R. Tagirov, and R. Tidecks, Full-switching FSF-type superconducting spin-triplet magnetic random access memory element, *Phys. Rev. B* **96**, 184521 (2017).
- [35] O. M. Kapran, A. Iovan, T. Golod, and V. M. Krasnov, Observation of the dominant spin-triplet supercurrent in Josephson spin valves with strong Ni ferromagnets. *Phys.*

- Rev. Research* **2**, 013167 (2020).
- [36] J. P. Cascales, Y. Takamura, G. M. Stephen, D. Heiman, F. S. Bergeret, and J. S. Moodera, Switchable Josephson junction based on interfacial exchange field. *Appl. Phys. Lett.* **114**, 022601 (2019).
 - [37] M. Weides, Magnetic anisotropy in ferromagnetic Josephson junctions, *Appl. Phys. Lett.* **93**, 052502 (2008).
 - [38] A. Iovan and V. M. Krasnov, Signatures of the spin-triplet current in a Josephson spin valve: A micromagnetic analysis. *Phys. Rev. B* **96**, 014511 (2017).
 - [39] I. A. Golovchanskiy, V. V. Bol'ginov, V. S. Stolyarov, N. N. Abramov, A. Ben Hamida, O. V. Emelyanova, B. S. Stolyarov, M. Yu. Kupriyanov, A. A. Golubov, and V. V. Ryazanov, Micromagnetic modeling of critical current oscillations in magnetic Josephson junctions, *Phys. Rev. B* **94**, 214514 (2016).
 - [40] M. A. E. Qader, R. K. Singh, S. N. Galvin, L. Yu, J. M. Rowell, N. Newman, Switching at small magnetic fields in Josephson junctions fabricated with ferromagnetic barrier layers. *Appl. Phys. Lett.* **104**, 022602 (2014).
 - [41] S.V. Bakurskiy, N.V. Klenov, I. I. Soloviev, M. Yu. Kupriyanov and A. A. Golubov, Superconducting phase domains for memory applications. *Appl. Phys. Lett.* **108**, 042602 (2016).
 - [42] S.V. Bakurskiy, N. V. Klenov, I. I. Soloviev, N. G. Pugach, M. Yu. Kupriyanov and A. A. Golubov, Protected $0 - \pi$ states in SISFS junctions for Josephson memory and logic. *Appl. Phys. Lett.* **113**, 082602 (2018).
 - [43] S. E. Shafraniuk, I. P. Nevirkovets and O. A. Mukhanov, Modeling Computer Memory Based on Ferromagnetic/Superconductor Multilayers. *Phys. Rev. Applied* **11**, 064018 (2019).
 - [44] N. Klenov, Y. Khaydukov, S. Bakurskiy, R. Morari, I. Soloviev, V. Boian, T. Keller, M. Kupriyanov, A. Sidorenko and B. Keimer, Periodic Co/Nb pseudo spin valve for cryogenic memory. *Beilstein J. Nanotechnol.* **10**, 833-839 (2019).
 - [45] K. R. Jeon, X. Montiel, S. Komori, C. Ciccarelli, J. Haigh, H. Kurebayashi, L. F. Cohen, A. K. Chan, K. D. Stenning, C. M. Lee, M. G. Blamire, and J. W. A. Robinson. *Phys. Rev. X* **10**, 031020 (2020).
 - [46] S.S.P. Parkin, N. More, and K.P. Roche, Oscillations in Exchange Coupling and Magnetoresistance in Metallic Superlattice structures: Co/Ru, Co/Cr, and Fe/Cr. *Phys. Rev. Lett.* **64**, 2304 (1990).
 - [47] D.H. Mosca, F. Petroff, A. Fert, P.A. Schroeder, W.P. Pratt Jr., and R. Laloe, Oscillatory interlayer coupling and giant magnetoresistance in Co/Cu multilayers. *J. Magn. Magn. Mat.* **94**, L1 (1991).
 - [48] F.J.A. den Broeder, W. Hoving, and P.J.H. Bloemen, Magnetic anisotropy of multilayers. *J. Magn. Magn. Mat.* **93**, 562 (1991).
 - [49] Details of simulation can be found in Ref. [44]. Note that in order to apply it to S2 ML, we have to assume a too small $\xi_S \simeq 5$ nm. Therefore Fig. 1 (c) only serves for a qualitative illustration of the proximity effect in such S/F heterostructure.
 - [50] A. Zeinali, T. Golod, and V. M. Krasnov, Surface superconductivity as the primary cause of broadening of superconducting transition in Nb films at high magnetic fields. *Phys. Rev. B* **94**, 214506 (2016).
 - [51] The measured Hall signal contains a small ($< 0.1\%$) admixture of the longitudinal resistance. In Fig. 1 (i) it was subtracted as described in T. Golod A. Rydh, and V. M. Krasnov, Anomalous Hall effect in NiPt thin films. *J. Appl. Phys.* **110**, 033909 (2011).
 - [52] A.V. Samoilov, A. Legris, F. Rullier-Albenque, P. Lejay, B. Bouffard, Z.G. Ivanov and L.-G. Johansson. Mixed-State Hall Conductivity in High- T_c Superconductors: Direct Evidence of Its Independence on Disorder *Phys. Rev. Lett.* **74** 2351 (1995).
 - [53] V. M. Krasnov and G.Yu. Logvenov, Selfconsistent analysis of Magnus and thermal forces acting on vortices in type-II superconductors. *Physica C* **274**, 286-294 (1997).
 - [54] E. B. Sonin, Magnus force in superfluids and superconductors. *Phys. Rev. B* **55**, 485-501 (1997).
 - [55] L. Embon, Y. Anahory, Ž.L. Jelić, E.O. Lachman, Y. Myasoedov, M.E. Huber, G.P. Mikitik, A.V. Silhanek, M.V. Milošević, A. Gurevich and E. Zeldov, Imaging of super-fast dynamics and flow instabilities of superconducting vortices. *Nature Commun.* **8**, 85 (2017).
 - [56] R. Laiho, E. Lähderanta, E. B. Sonin, and K. B. Traito, Penetration of vortices into the ferromagnet/type-II superconductor bilayer. *Phys. Rev. B* **67**, 144522 (2003).
 - [57] V. K. Vlasko-Vlasov, U. Welp, A. Imre, D. Rosenmann, J. Pearson, and W. K. Kwok, Soft magnetic lithography and giant magnetoresistance in superconducting/ferromagnetic hybrids. *Phys. Rev. B* **78**, 214511 (2008).
 - [58] A. Yu. Aladyshkin, A. V. Silhanek, W. Gillijns and V. V. Moshchalkov, Nucleation of superconductivity and vortex matter in superconductor/ferromagnet hybrids. *Supercond. Sc. Technol.* **22**, 053001 (2009).
 - [59] M. Iavarone, A. Scarfato, F. Bobba, M. Longobardi, G. Karapetrov, V. Novosad, V. Yefremenko, F. Giubileo, and A. M. Cucolo, Imaging the spontaneous formation of vortex-antivortex pairs in planar superconductor/ferromagnet hybrid structures. *Phys. Rev. B* **84**, 024506 (2011).
 - [60] F. Béron, D. Ménard, and A. Yelon, First-order reversal curve diagrams of magnetic entities with mean interaction field: A physical analysis perspective. *J. Appl. Phys.* **103**, 07D9088 (2008).
 - [61] C.-I. Dobrotă and A. Stancu, What does a first-order reversal curve diagram really mean? A study case: Array of ferromagnetic nanowires. *J. Appl. Phys.* **113**, 043928 (2013).
 - [62] R. K. Dumas, P. K. Greene, D. A. Gilbert, L. Ye, C. Zha, J. Åkerman, and K. Liu, Accessing different spin-disordered states using first-order reversal curves. *Phys. Rev. B* **90**, 104410 (2014).